metals

MDPI

Article

Effect of Laser Cladding Stellite 6-Cr_3C_2-WS_2 Self-Lubricating Composite Coating on Wear Resistance and Microstructure of H13

Wei Chen *, Bo Liu, Long Chen, Jiangping Xu and Yingxia Zhu

School of Mechanical Engineering, Jiangsu University, Zhenjiang 212013, China; 2221803031@stmail.ujs.edu.cn (B.L.); xianglongjiubian@outlook.com (L.C.); jiangpingxu@ujs.edu.cn (J.X.); xia166109@163.com (Y.Z.)

* Correspondence: chen_wei@ujs.edu.cn; Tel.: +86-511-8879-1795

Received: 26 April 2020; Accepted: 8 June 2020; Published: 13 June 2020

Abstract: In order to prevent the wear failure of the hot-working die, the composite coatings of Stellite 6-Cr_3C_2-WS_2 was fabricated on H13 hot-working die steel by laser cladding. The composite coating was prepared through the in-situ generation technology, that can give H13 the ability of self-lubricating at the working temperature (about 200 °C). The effect of the various WS_2 percentages on the properties of the coating was studied by X-ray diffraction (XRD), scanning electron microscopy (SEM), energy dispersive spectroscopy (EDS), microhardness test, friction and wear test. In addition, the phase constitutions, microstructures and wear properties were also investigated systematically. The obtained hardness of the cladding coating is approximately 2.5 times higher than the substrate because of the constituents of γ-(Fe, Co)/Cr_7C_3 eutectic colony, (Cr, W)C carbide and dendritic crystals in the coating. Furthermore, the friction coefficient decreases to 70% of the substrate due to the CrS self-lubricating phase. The analyses results suggest that an 85% Stellite 6-10% Cr_3C_2-5% WS_2 composite coating has excellent material properties.

Keywords: self-lubricating effect; composite coating; laser cladding; H13 steel

1. Introduction

Due to the excellent high-temperature resistance, high strength and oxidation resistance, H13 steel has been widely used in hot-working die, casting die and extrusion die [1–3]. Unfortunately, the intense friction in the deformation of sheet metal can result in cracks and fatigue wear on H13 steel in the hot stamping process [4–6]. In order to improve the surface properties, composite coating has been adopted on the die surface with poor wear resistance [7,8]. Adding alloy powder with the similar chemical composition into the base material can ensure an excellent metallurgical bonding interface. As a competitive and effective surface strengthening technique, laser cladding can produce microstructure with fine and even crystals, thereby the mechanical properties of the coating are improved [9–13]. Compared with the traditional technology of improving surface properties, the laser cladding exhibits many outstanding advantages, such as concentrated heat input, short processing time, fast coating cooling, low dilution ratio of the cladding layer, good metallurgical combination of substrate and cladding coatings, wide selective range of laser cladding powder, and so on [14–17]. In addition, the in-situ self-lubricating method is one of the methods used to generate the lubricating phase [18–20]. As compared to the directly added lubricating phase, the advantages of the in-situ self-lubricating are obvious, such as avoiding poor bonding performance and cracking between the directly added lubricating phase and the coatings. Thus, many researchers have conducted studies on laser cladding using in-situ self-lubricating technology to improve the surface properties of materials [21,22]. Currently,

much attention has been paid to laser cladding self-lubricating wear-resistant composite coating which has become one of the most studied areas of improving material surface properties. Li et al. [23] studied the preparation of Fe-based composite coatings with Cr_3C_2/MoS_2 particles on the 45# steel. Their results indicated that the main phases of the coating were CrS, $Cr_{23}C_6$ and MoS_2 and the coating fabricated by in-situ self-lubricating had excellent wear resistance. In addition, the friction coefficient of cladding coatings decreased significantly by 51% of that of the substrate, and the wear resistance was remarkably improved. Chen et al. [24] conducted a study on the Co-based coating by adding different amounts of NbC and h-BN on the Cr12MoV. The main phases of the cladding coating were Nb(C,B). Their result showed that, as compared to the substrate, the hardness of the cladding coating increased by 2–3 times, and the friction coefficient of coatings also descended significantly. Li et al. [25] investigated the preparation of self-lubricating phase coating on 35CrMo steel by a composite of Co-based powder and adding Ti_3SiC_2. It was found that the main phases of the coating were γ-Co, Cr_7C_3 and Ti_3SiC_2. In addition, their study results showed that the hardness of the coating was 2–3 times that of the substrate and the wear resistance was greatly improved due to the existence of the self-lubricating phase. Torres et al. [26] utilized the Ag/MoS_2-based self-lubricating cladding on aluminum alloy AA6082 to get Cr_2S_3, Cr_3S_4 and NiS_2 in the self-lubricating phase. The hardness of the cladding coating increased by 2 times, and the friction coefficient of coatings also decreased by 55% of that of the substrate. Piasecki et al. [27] studied the self-lubricating boride layers on Inconel 600-alloy by laser cladding and found that the coatings included dendritic and globular precipitates of nickel, chromium and iron borides among the soft Ni–phase. The friction coefficient of coatings decreased remarkably. Nghia et al. [28] investigated the microstructure and properties of Cu/TiB_2 composite coatings on H13 steel by in-situ laser cladding. The results showed that the main phase of coatings was Cu, Ti, Fe and $TiFe_3$. The surface hardness of coatings was significantly higher than that of the substrate. The wear resistance of the coatings was also better than that of the substrate. Cui et al. [29] produced self-lubricated oxide-containing tribo-coatings by adding the particles of MoS_2 and Fe_2O_3. It was found that because of the mixed additives of MoS_2 and Fe_2O_3, the protective tribo-coatings presented a load-carrying capability and lubricative function. However, some common composite coatings could not suit the industrial application requirements of H13, such as high hardness and wear resistance at high working temperatures. Therefore, the self-lubricating anti-wear coating on the die surface by laser cladding was used to improve the performance of H13 in this research.

To improve the hardness and wear resistance of H13, powders with different proportions of Stellite 6-Cr_3C_2-WS_2 were designed and were used to cover the surface of H13 steel by laser cladding. Then, the effect of different WS_2 additions on a Co-based composite coating were analyzed on the microhardness, wear resistance, microstructure, wear mechanism and self-lubricating ability. This paper aims at improving the hardness and wear resistance on H13 and providing essentials for the application of the self-lubricating coatings.

2. Materials and Methods

In this paper, the H13 steel which is often used in high temperature conditions, was chosen as the substrate and its chemical compositions are shown in the third row of Table 1. The dimension size of the substrate was 50 mm × 20 mm × 10 mm, covered by a laser cladding surface with a size of 50 mm × 20 mm. According to the order of gravel size, the sandpaper was used to clean the substrate surface from dust and oxide film. Then alcohol was used to remove the oil on the surface of the substrate. In order to obtain the high hardness and great wear resistance of the cladding coatings, Co-based powder, such as Stellite 6 (Kennametal Stellite Co., Ltd., Shanghai, China), was adopted for the coatings (see the chemical compositions of Stellite 6 in the fourth row of Table 1). In addition, three kinds of composite powders with different mass percentages of Stellite 6, Cr_3C_2 and WS_2 were prepared and used in the laser cladding. The purity of Cr_3C_2 (Aidun Co., Ltd., Heibei, China) and WS_2 (Shanghai Onway Co., Ltd., Shanghai, China) are 99.9%. Then the corresponding three specimens were made from the substrates and coatings, as shown in Table 2.

Table 1. Chemical compositions of H13 hot working die and Stellite 6.

Material	Element (wt%)							
	C	**Si**	**Mn**	**Cr**	**Mo**	**V**	**Co**	**Fe**
H13	0.40	1.00	0.30	5.15	1.35	1.10	-	Bal.
Stellite 6	1.15	1.10	0.05	29.00	1.00	-	Bal.	3.00

Table 2. Compositions of different specimens.

No.	Specimen 1	Specimen 2	Specimen 3
Substrate	H13	H13	H13
Coating	90% Stellite 6-10% Cr_3C_2 composite coatings	85% Stellite 6-10% Cr_3C_2-5% WS_2 composite coatings	80% Stellite 6-10% Cr_3C_2-10% WS_2 composite coatings

The proportioned powder as shown in Table 2 was ground by a speed of 300 r/min in a QM-3SP2 planetary mill (Nanjing Chi Shun Technology Development Co., Ltd., Nanjing, China) for 2 hours and then dried at a temperature of 200 °C for 1 h before laser cladding. The powders were fed to the substrate surface by side axis method and then melted by a LDM3000-60 semiconductor laser (Laserline GmbH, Mülheim-Kärlich, Germany). During the laser cladding test, these processing parameters were selected: laser power 1600 W, scanning speed 400 mm/min, powder feeding amount 12 L/min, spot diameter 4 mm, wavelength 900 nm and protective gas nitrogen. Thus, good quality coatings were achieved with those parameters. To avoid cracks on the surface during laser cladding, the substrate H13 was preheated.

After the laser cladding process, the specimens were crosscut and metallographic specimens were prepared following standard mechanical polishing procedures. The phase constituents of cladding coatings were analyzed by a D8-Advance X-ray diffractometer (Bruker AXS GmbH, Karlsruhe, Germany) at a scanning speed of 5 °/min ranging from 20° to 100° with Cu target Kα radiation, and accelerating voltage of 40 kV and a current of 40 mA; the microstructure and element of cladding coatings were identified by a S-3400N scanning electron microscope equipped with an X-ray spectrometer (JEOL, Tokyo, Japan); the microhardness of cladding coatings was also measured using an HV-1000 hardness tester (Suzhou Jingli Co., Ltd., Suzhou, China) with a test load of 300 g and a dwell time of 15 s. Moreover, the wear resistance of cladding coatings was measured by a MFT-5000 multi-functional friction and wear machine (Rtec GmbH, San Jose, CA, USA). The coupled ball is GCr15 steel (ø9.5 mm) and the corresponding rotating speed, loading force, wearing time, and working temperature of hot die were 25 r/min, 50 N, 60 min, and 25 °C/200 °C, respectively. The weight loss of the specimen was measured by an electronic balance whose precision was 0.1 mg (Bond West Instrument Technology Co., Ltd., Shanghai, China) and the worn morphology was observed by an optical microscope (Olympus GmbH, Tokyo, Japan).

3. Results and Discussion

3.1. Constituent Phase and Microstructure

The cross section of the Co-based composite coatings 1–3 are shown in Figure 1, in which the bonding line between the substrate and coating could be observed. The cladding coatings are uniform, smooth and free of defects such as pores and impurities. The good metallurgical combination is obtained between the cladding coating and the substrate, because the bonding line is stable and of low dilution ratio.

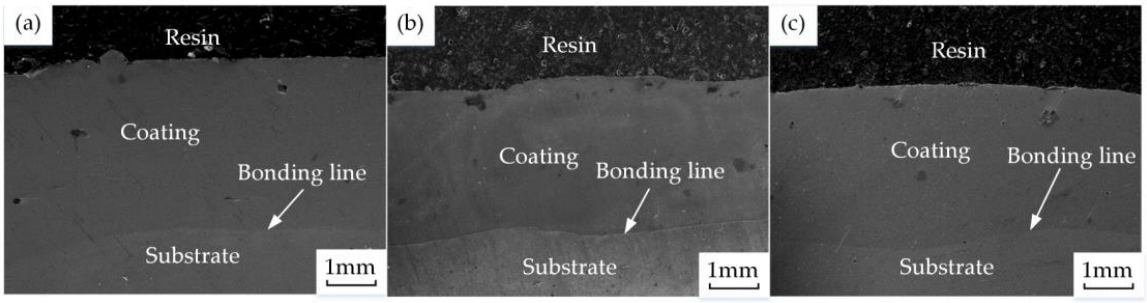

Figure 1. The cross section of the coatings 1–3: (**a**) coating 1; (**b**) coating 2; (**c**) coating 3.

The XRD diffraction patterns of coatings from specimens 1, 2 and 3 are shown in Figure 2. The phases of specimen 1 mainly consist of γ-(Fe, Co), Cr_7C_3, Cr_3C_2 and other carbides. The main chemical reactions are described in Equations (1)–(4). WS_2 and Cr_3C_2 decompose under high temperature [30,31]. The S and C elements react with Cr to form CrS and Cr_7C_3, respectively. The hard phases γ-(Fe, Co) and Cr_7C_3 mainly contribute to improve the hardness of the cladding coatings. Besides this, no oxides are generated in the cladding coatings because of the good self-fusibility of the Co-based alloy powder. Compared to specimen 1, specimens 2 and 3 generate the extra phases of CrS, (Cr, W)C and WS_2 due to the addition of WS_2 in the cladding powder. The (Cr, W)C carbides and CrS self-lubricating phase is generated due to the decomposition of WS_2 at 450 °C and the reaction. The lubricating property and wear resistance are improved because of the CrS and residual WS_2.

$$WS_2 \xrightarrow{\Delta} W + 2S \quad (1)$$

$$Cr_3C_2 \xrightarrow{\Delta} 3Cr + 2C \quad (2)$$

$$Cr + S \rightarrow CrS \quad (3)$$

$$7Cr + 3C \rightarrow Cr_7C_3 \quad (4)$$

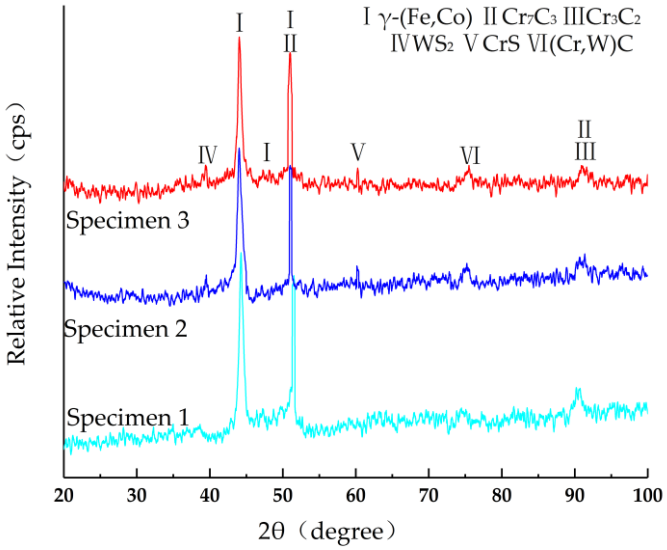

Figure 2. X-ray diffraction diagrams of different specimen coatings.

Figure 3 shows the microstructures in the cladding coating of specimens 1–3. The grains at the bottom region in Figure 3a,d,g are mainly plane crystals which are fine and uniform, and the grains closest to the substrate are denser and smaller. According to the solidification theory, the solidification

always goes forward with the liquid–solid interface in the whole cooling crystallization process. The initial crystallization takes place at the solid-phase substrate where the temperature gradient (temperature/solidification rate) of the coating near the substrate is relatively large [32]. The dendrite epitaxial growth has a strong directionality and the plane crystal grows vertically to the substrate.

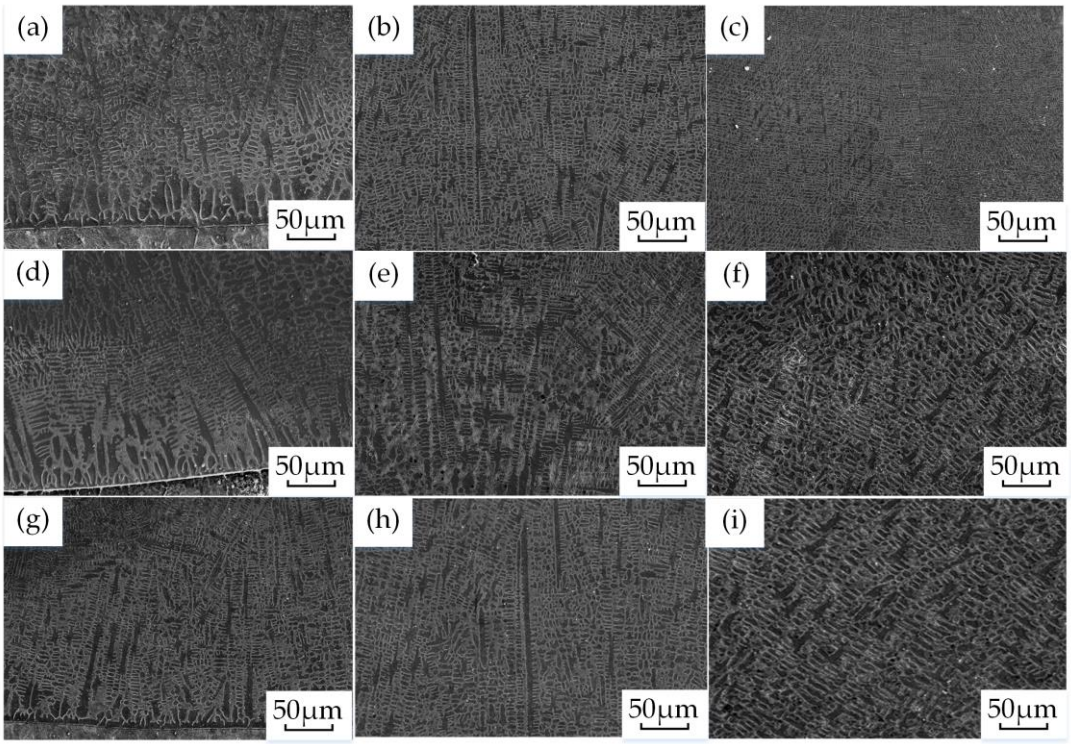

Figure 3. SEM images of specimens 1–3 of the cladding coating: (**a**) at bottom region of specimen 1; (**b**) at middle region of specimen 1; (**c**) at top region of specimen 1; (**d**) at bottom region of specimen 2; (**e**) at middle region of specimen 2; (**f**) at top region of specimen 2; (**g**) at bottom region of specimen 3; (**h**) at middle region of specimen 3; (**i**) at top region of specimen 3.

As shown in Figure 3b,e,h the plane crystals turn into dendrite crystals in the middle region because of the gradual increase of the grain growth rate as a result of the increase in temperature and decrease in solidification speed. The crystals initially grow vertically to the interface between coating and substrate and then grow into dendrites in the middle of the coating due to the non-directional heat dissipation. The top of the cladding coating is shown in Figure 3c,f,i. It is full of cellular grains because the heat dissipation at the top region of the coating under high temperature is slow and then nucleation has sufficient time to grow cellular crystals.

For comparison, the microstructures in the middle region of specimens 1–3 are shown in Figure 4. During the laser cladding, the crystals precipitated in the welding pool and then grew into dendrites. The dendrite and intergranular network eutectic structure are generated due to the eutectic reaction in the transformation of the intergranular metal solution to the solid-state. The microstructures at the middle regions of cladding coatings of specimens 2 and 3 are more compact and uniform than that of specimen 1 because of the high thermal conductivity of the cladding coatings with WS_2. The grains could refine when the growth rate of grains is less than the nucleating rate. Moreover, the high absorption capacity of the laser beam on the W element results in better energy conversion and then improves the combination between coating and substrate.

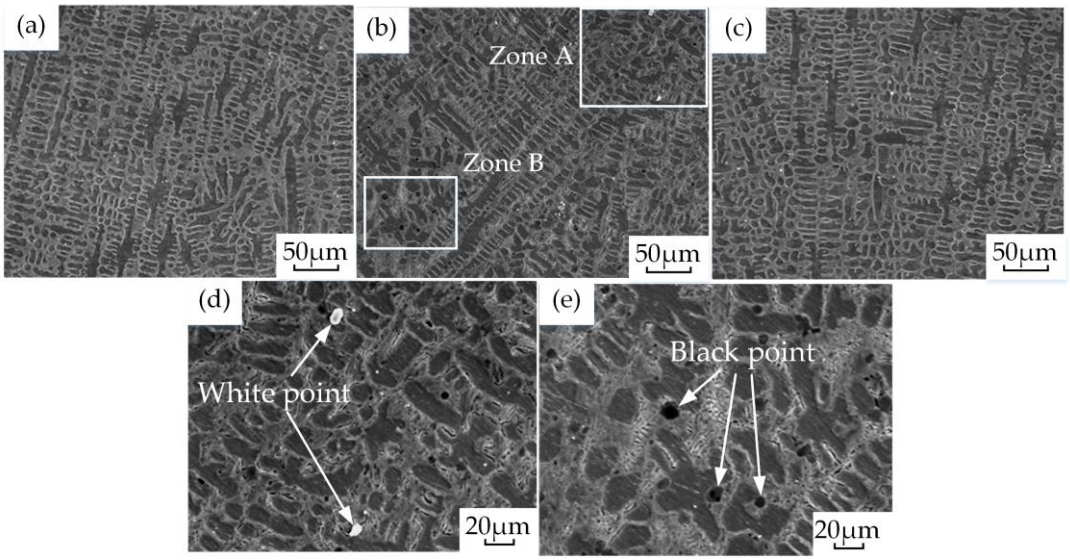

Figure 4. SEM images of middle region of specimen 1–3: (**a**) specimen 1; (**b**) specimen 2; (**c**) specimen 3; (**d**) zoomed zone A; (**e**) zoomed zone B.

In addition, white point in zone A and black point in zone B are found in Figure 4b. The element compositions of the white point in zone A and black point in zone B are analyzed by EDS analysis and indicated in Table 3. The white point is hard phase carbide, which consists of Cr_7C_3 and Cr_3C_2, and the black point is the lubricating phase that is CrS, which are consistent with the results from XRD analysis.

Table 3. EDS results of laser cladding coatings in zone A and zone B.

Point	Composition (wt%)					
	Co	C	Cr	S	W	Mn
White point	7.21	27.37	57.71	-	-	5.17
Black point	1.10	1.92	56.71	38.28	1.63	0.36

3.2. Microhardness

The microhardness variations along different coating depths in the three specimens are plotted in Figure 5. The microhardness in the three specimens are approximately 2.5 times that of the substrate and exhibit three distinguishable zone: zones I, II, and III. The microhardness in zone I decreases slightly with increasing depths and seems stable due to the evenly distributed materials in the laser cladding region. While in the narrow bonding region II, the microhardness increases with a big jump due to the following two reasons: at first, the grains in the bonding zone are refined and dendritic because of rapid temperature fluctuation in the laser cladding; secondly, the γ-(Fe, Co) is generated by the diffusion of Fe element from the substrate to the bonding zone and the amount of hard carbide (Cr, W)C in the region. In zone III, the microhardness decreases rapidly because of more plane crystals, less dendrites and much less carbide in the deeper region. The average microhardness of specimens 1, 2 and 3 are 556 ± 10 HV, 527 ± 12 HV and 516 ± 11 HV, respectively, which are all around 2.5 times that of the substrate (215 HV ± 15 HV). This is caused by the solution and dispersion strengthening resulting from the dissolution of Cr and C atoms in the Co-phase. The microhardness of specimen 1 is higher than that of specimens 2 and 3 due to the amount of Cr_7C_3 in the coatings.

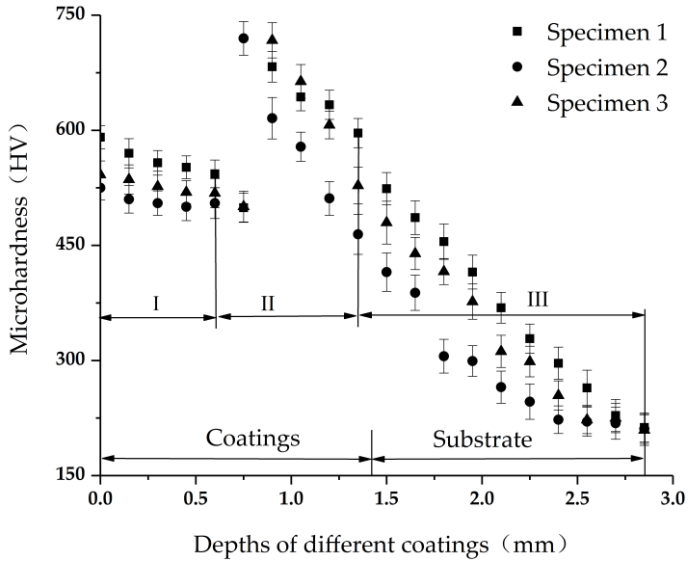

Figure 5. Microhardness of cladding coatings of different specimens.

3.3. Friction Coefficient and Weight Loss

The evolutions of friction coefficients obtained from the three specimens and the substrate at a room temperature of 25 °C are plotted in Figure 6a. Overall, the friction coefficients of the specimens reduce by 20–25%. This is because of the presence of Cr_7C_3 in specimen 1 and the continuous and uniform lubricating film generated by WS_2 powder in specimens 2 and 3. The friction coefficients in all of the four cases initially increase rapidly and then tend to be stable after 200 s, and the coefficient of the substrate fluctuated between 0.35 and 0.4 due to the insufficient hardness and coarse surface. We also notice that the friction coefficient of specimen 2 is smaller and more stable than that of specimen 1 and specimen 3 because of more self-lubricating phases and hard phases generated.

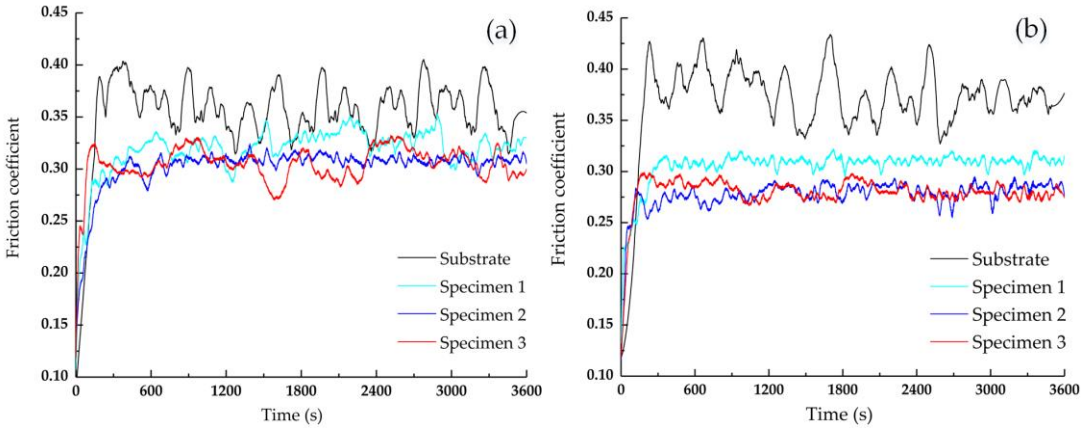

Figure 6. Evolutions of friction coefficients from different specimens at different temperatures: (**a**) at 25 °C; (**b**) at 200 °C.

The evolutions of corresponding friction coefficients in all the four cases at 200 °C are also plotted, as shown in Figure 6b. The friction coefficients are smaller and more stable than those at 25 °C in Figure 6a due to the fact that more CrS separated at high temperature can act as the lubricant. In addition, the friction coefficient of specimen 2 is approximately 0.26–0.28, just 70% of that of the substrate, and its evolution curve is more stable than that of specimen 3 because of the excessive S element from the decomposition of WS_2 under laser irradiation.

The wear weight loss of the three specimens and the substrate at 25 °C and 200 °C are both demonstrated in Figure 7. The loss of the three specimens are significantly less than that of the substrate due to the solid solution strengthening effect of γ-(Fe, Co) and the improved wear resistance of hard phase Cr_7C_3. In addition, the wear weight loss of specimens 2 and 3 are smaller than that of specimen 1, suggesting that WS_2 and CrS play the critical role of producing lubrication film and reducing wear, especially at 200 °C.

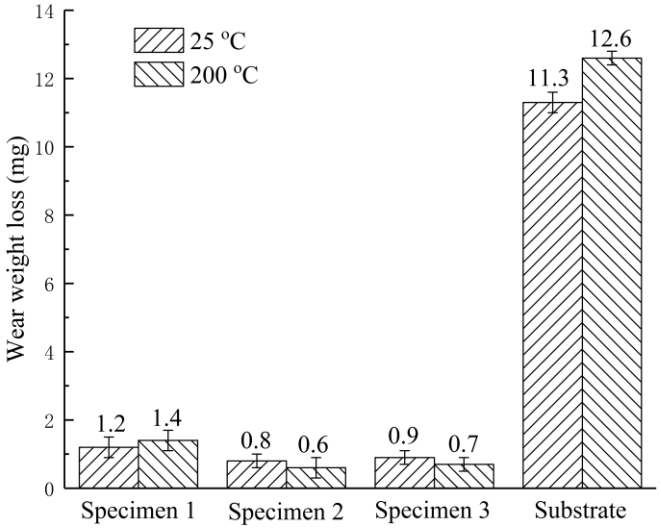

Figure 7. Wear weight loss of different coatings at different temperatures.

3.4. Wear Mechanism

Wear mechanism plays a significant role of changing the friction coefficient and wear weight loss, and was studied deeply in the three specimens. Figure 8 shows the wear surface morphology of the three specimens and the substrate at 25 °C. In Figure 8a, large numbers of block shedding and deep furrow caused by low hardness of the substrate and absence of the hard phase led to serious abrasive wear and adhesive wear on the substrate surface. In contrast, the coating surfaces in the three specimens in Figure 8b–d observed with shallow scratching and small plastic deformation are almost smooth and flat as a result of the mild abrasive and adhesive wear. In the wear process, the soft phase structure was removed at the initial stage. Since the contact stress between the grinding ball and the hard phase is beyond the yield limit of the hard phase, the hard phase particles drop off and act as abrasive particles in the process. The remaining hard phase effectively resists wear, deformation and scratches. In specimen 3, the white areas pointed to by arrows, shown in Figure 8d, mainly include elements of C, Cr and W observed by EDS analysis, and consist of (Cr, W)C carbides according to the XRD analysis. Therefore, the material surface, effectively protected by the (Cr, W)C carbides is hard to be worn.

The wear morphologies of specimens 1–3 and the substrate at 200 °C are also demonstrated in Figure 9a–d, respectively. The wear surface of the substrate and specimen 1 was seriously damaged without the protection of lubrication film at 200 °C. The surfaces of specimens 2 and 3 are almost smooth and with few slight scratches. Besides this, many black regions on the wear surface include large numbers of self-lubricating phases of WS_2/CrS obtained by energy spectrum analysis and XRD analysis. Hence, the self-lubricating phase CrS that separated at a high temperature acts as the lubricating film at the contact surfaces to reduce the friction coefficient. It results in mild abrasive and adhesive wear on the contact surfaces. In addition, there is less plastic deformation and furrow on the surface than those in the case of 25 °C.

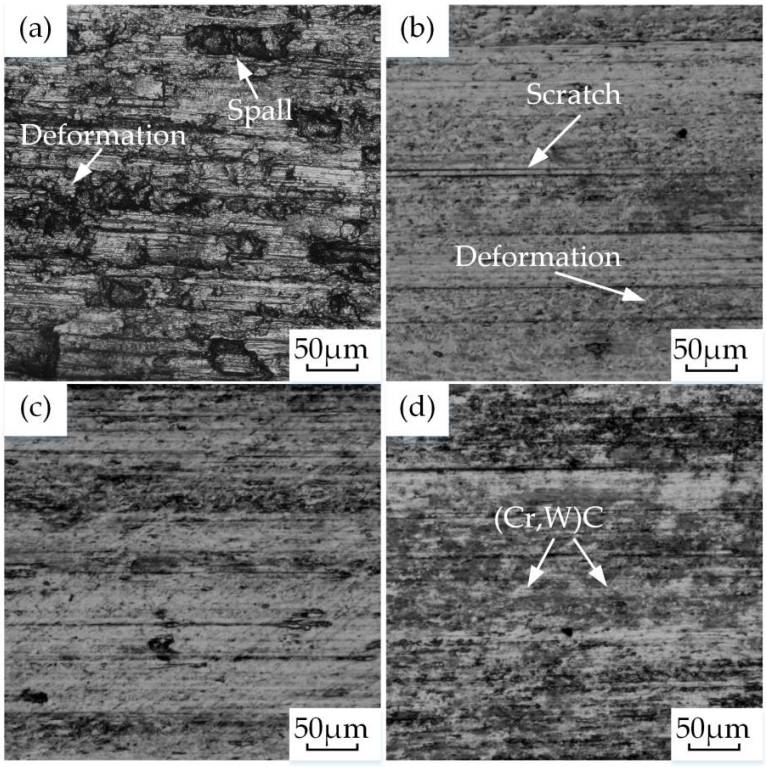

Figure 8. Optical micrographs of wear surface morphology at 25 °C: (**a**) the substrate; (**b**) specimen 1; (**c**) specimen 2; (**d**) specimen 3.

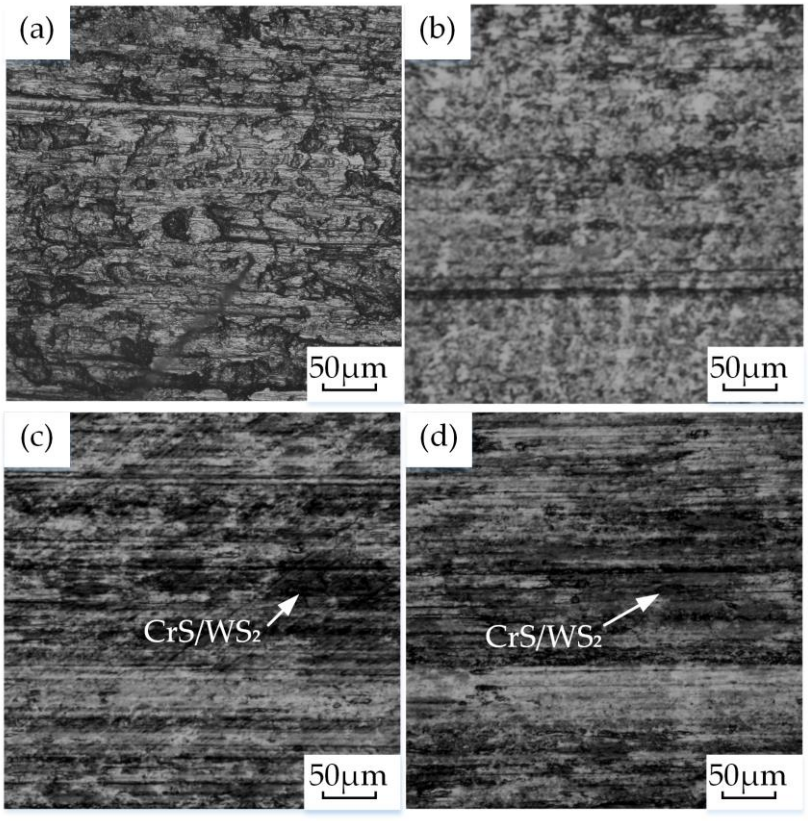

Figure 9. Optical micrographs of wear surface morphology at 200 °C: (**a**) the substrate; (**b**) specimen 1; (**c**) specimen 2; (**d**) specimen 3.

4. Conclusions

To improve the hardness and wear resistance of H13, different proportions of composite powder were covered on the surface of H13 steel by laser cladding. The microstructure, hardness, and wear resistance of different laser cladding coatings on H13 were investigated. The main conclusions are summarized as following:

1. The Stellite 6-Cr_3C_2-WS_2 laser cladding coating mainly consists of hard phases γ-(Fe, Co), Cr_7C_3 and Cr_3C_2, self-lubricating phase CrS and residual WS_2. The obtained coating without cracks and pores demonstrates good metallurgical combination with the substrate.
2. The hardness of laser cladding coatings is 2–3 times higher than that of the substrate due to the generation of γ-Co saturated solution and (Cr, W)C carbide hard phase.
3. The laser cladding coating on the substrate reduces the friction coefficient to 70% of the substrate at 200 °C. In particular, the generation of the self-lubricating phase CrS at 200 °C acts as the lubricating film on the contact surface, thus produces less wear weight loss than that observed at 25 °C.
4. The change of wear mechanism in cladding coatings remarkably reduces the degree of abrasive wear and adhesive wear due to the presence of hard phase and self-lubricating phase in the coatings.
5. The 85% Stellite 6-10% Cr_3C_2-5% WS_2 laser cladding coating provided good anti-wear properties and self-lubricating ability at 200 °C. The friction coefficient of specimen 2 was 0.26–0.28, and the wear weight loss was 0.6 mg.

Author Contributions: Conceptualization, W.C.; methodology, investigation, resources, formal analysis and writing—original draft preparation, B.L.; validation, writing—review and editing, L.C., J.X. and Y.Z.; supervision, W.C.; project administration, funding acquisition, W.C. All authors have read and agreed to the published version of the manuscript.

Funding: This research was funded by the National Natural Science Foundation of China, No. 51875263; Postgraduate Research and Practice Innovation Program of Jiangsu Province, No. SJCX19_0545.

Acknowledgments: The authors would also like to thank the Laboratory of Advanced Forming Institute, and the Analysis and Testing Center of Jiangsu University.

Conflicts of Interest: The authors declare no conflict of interest. The funders had no role in the design of the study; in the collection, analyses, or interpretation of data; in the writing of the manuscript, or in the decision to publish the results.

References

1. Zang, C.L.; Zhou, T.; Zhou, H.; Yuan, Y.H.; Zhang, P.; Meng, C.; Zhang, Z.H. Effects of substrate microstructure on biomimetic unit properties and wear resistance of H13 steel processed by laser remelting. *Opt. Laser Technol.* **2018**, *106*, 299–310. [CrossRef]
2. Koneshlou, M.; Asl, K.M.; Khomamizadeh, F. Effect of cryogenic treatment on microstructure, mechanical and wear behaviors of AISI H13 hot work tool steel. *Cryogenics* **2011**, *51*, 55–61. [CrossRef]
3. Chen, L.; Chen, W.; Xu, F.; Zhu, Y.X.; Zhu, Y.T. A pre-design method for drilled cooling pipes in hot stamping tool based on pipe parameter window. *Int. J. Adv. Manuf. Technol.* **2019**, *103*, 891–900. [CrossRef]
4. Girisha, V.A.; Joshi, M.M.; Kirthan, L.J.; Bharatish, A. Thermal fatigue analysis of H13 steel die adopted in pressure-die-casting process. *Sādhanā* **2019**, *44*, 148. [CrossRef]
5. Wang, M.; Wu, Y.; Wei, Q.S.; Shi, Y.S. Thermal Fatigue Properties of H13 Hot-Work Tool Steels Processed by Selective Laser Melting. *Metals* **2020**, *10*, 116. [CrossRef]
6. Ning, A.G.; Mao, W.W.; Chen, X.C.; Guo, H.J.; Guo, J. Precipitation behavior of carbides in H13 hot work die steel and its strengthening during tempering. *Metals* **2017**, *7*, 70. [CrossRef]
7. Wang, G.Y.; Zhang, J.Z.; Shu, R.Y.; Yang, S. High temperature wear resistance and thermal fatigue behavior of Stellite6/WC coatings produced by laser cladding with Co-coated WC powder. *Int. J. Refract. Met. Hard Mater.* **2019**, *81*, 63–70. [CrossRef]

8. Yan, H.; Zhang, J.; Zhang, P.L.; Yu, Z.S.; Li, C.G.; Xu, P.Q.; Lu, Y.L. Laser cladding of Co-based alloy/TiC/CaF_2 self-lubricating composite coatings on copper for continuous casting mold. *Surf. Coat. Technol.* **2013**, *232*, 362–369. [CrossRef]
9. Telasang, G.; Majumdar, J.D.; Padmanabham, G.; Manna, M.T. Effect of laser para-meters on microstructure and hardness of laser clad and tempered AISI H13 tool steel. Surf. *Coat. Technol.* **2014**, *258*, 1108–1118. [CrossRef]
10. Liu, M.; Qin, Z.H.; Yang, X.Q.; Lin, Z.; Guo, T. Fabricating controllable hierarchical pores on smooth carbon sheet for synthesis of supercapacitor materials. *Vacuum* **2019**, *168*, 108806. [CrossRef]
11. Kong, L.; Guo, Y.; Wang, X.; Zhang, X. Double-walled hierarchical porous silica nanotubes loaded Au nanoparticles in the interlayer as a high-performance catalyst. *Nanotechnology* **2019**, *31*, 015701. [CrossRef] [PubMed]
12. Dervaux, J.; Cormier, P.A.; Konstantinidis, S.; Ciuccio, R.D.; Coulembier, O.; Dubois, P.; Snyders, R. Deposition of porous titanium oxide thin films as anode material for dye sensitized solar cells. *Vacuum* **2015**, *114*, 213–220. [CrossRef]
13. Peyre, P. Additive layer manufacturing using metal deposition. *Metals* **2020**, *10*, 459. [CrossRef]
14. Knoop, D.; Lutz, A.; Mais, B.; Hehl, A.V. A tailored AlSiMg alloy for laser powder bed fusion. *Metals* **2020**, *10*, 514. [CrossRef]
15. Li, C.G.; Zeng, M.; Liu, C.M.; Wang, F.F.; Guo, Y.J.; Wang, J.Q.; Yang, Y.; Li, W.G.; Wang, Y. Microstructure and tribological behavior of laser cladding TiAlSi composite coatings reinforced by alumina–titania ceramics on Ti6Al4V alloys. *Mater. Chem. Phys.* **2020**, *240*, 122271. [CrossRef]
16. Mostajeran, A.; Shoja-Razavi, R.; Hadi, M.; Erfanmanesh, M.; Barekat, M.; Firouzabadi, M.S. Evaluation of the mechanical properties of WC-FeAl composite coating fabricated by laser cladding method. *Int. J. Refract. Met. Hard Mater.* **2020**, *88*, 105199. [CrossRef]
17. Li, M.; Han, B.; Song, L.; He, Q. Enhanced surface layers by laser cladding and ion sulfurization processing towards improved wear-resistance and self-lubrication performances. *Appl. Surf. Sci.* **2020**, *503*, 144226. [CrossRef]
18. Ke, J.; Liu, X.B.; Liang, J.; Liang, L.; Yang, S.L. Microstructure and fretting wear of laser cladding self-lubricating anti-wear composite coatings on TA2 alloy after aging treatment. *Opt. Laser Technol.* **2019**, *119*, 105599. [CrossRef]
19. Zhang, P.L.; Zhao, G.P.; Wang, W.W.; Wang, B.; Shi, P.Y.; Qi, G.; Yi, G.W. Study on the Mechanical and Tribological Properties and the Mechanisms of Cr-Free Ni-Based Self-Lubricating Composites at a Wide Temperature Range. *Metals* **2020**, *20*, 268. [CrossRef]
20. Mi, P.B.; Ye, F.X. Wear performance of the WC/Cu self-lubricating textured coating. *Vacuum* **2018**, *157*, 17–20. [CrossRef]
21. Torres, H.; Vuchkov, T.; Slawik, S.; Gachot, C. Self-lubricating laser claddings for reducing friction and wear from room temperature to 600 °C. *Wear* **2018**, *408*, 22–33. [CrossRef]
22. Torres, H.; Slawik, S.; Gachot, C.; Prakash, B.; Rodríguez Ripoll, M. Microstructural design of self-lubricating laser claddings for use in high temperature sliding applications. *Surf. Coat. Technol.* **2018**, *337*, 24–34. [CrossRef]
23. Li, A.N.; Wei, C.J.; Liu, J.J.; Zhou, W.L.; Wang, H.J.; Shi, S.D. Microstructure and tribological properties of laser cladding iron base Cr_3C_2/MoS_2 cladding. *China Surf. Eng.* **2015**, *28*, 77–85.
24. Chen, Z.F.; Yan, H.; Zhang, P.L.; Yu, Z.H.; Lu, Q.H.; Guo, J.L. Microstructural evolution and wear behaviors of laser-clad Stellite 6/NbC/h-BN self-lubricating coatings. *Surf. Coat. Technol.* **2019**, *372*, 218–228. [CrossRef]
25. Li, X.; Zhang, C.H.; Zhang, S.; Wu, C.L.; Liu, Y.; Zhang, J.B.; Shahzad, M.B. Manufacturing of Ti3SiC2 lubricated Co-based alloy coatings using laser cladding technology. *Opt. Laser Technol.* **2019**, *114*, 209–215. [CrossRef]
26. Torres, H.; Caykara, T.; Rojacz, H.; Prakash, B.; Rodríguez Ripoll, M. The tribology of Ag/MoS_2-based self-lubricating laser claddings for high temperature forming of aluminium alloys. *Wear* **2020**, *203110*. [CrossRef]
27. Piasecki, A.; Kotkowiak, M.; Makuch, N.; Kulka, M. Wear behavior of self-lubricating boride layers produced on Inconel 600-alloy by laser alloying. *Wear* **2019**, *426*, 919–933. [CrossRef]
28. Nghia, T.V.; Sen, Y.; Anh, P.T. Microstructure and properties of Cu/TiB2 wear resistance composite coating on H13 steel prepared by in-situ laser cladding. *Opt. Laser Technol.* **2018**, *108*, 480–486.

29. Cui, X.H.; Jin, Y.X.; Chen, W.; Zhang, Q.Y.; Wang, S.Q. Improvement of tribological performance of AISI H13 steel by means of a self-lubricated oxide-containing tribo-layer. *J. Mater. Eng. Perform.* **2018**, *27*, 1945–1956. [CrossRef]
30. Yang, M.S.; Liu, X.B.; Fan, J.W.; He, X.M.; Shi, S.H.; Fu, G.Y.; Wang, M.D.; Chen, S.F. Microstructure and wear behaviors of laser clad NiCr/Cr_3C_2-WS_2 high temperature self-lubricating wear-resistant composite coating. *Appl. Surf. Sci.* **2012**, *258*, 3757–3762. [CrossRef]
31. Cui, S.; Li, W.S.; He, L.; Feng, L.; An, G.S.; Hu, W.; Hu, C.X. Tribological behavior of a Ni-WS_2 composite coating across wide temperature ranges. *Rare Met.* **2019**, *38*, 1078–1085. [CrossRef]
32. Lu, J.Z.; Cao, J.; Lu, H.F.; Zhang, L.Y.; Luo, K.Y. Wear properties and microstructural analyses of Fe-based coatings with various WC contents on H13 die steel by laser cladding. *Surf. Coat. Technol.* **2019**, *369*, 228–237. [CrossRef]